

Electric Control of Spin Transitions at the Atomic Scale

Piotr Kot,¹ Maneesha Ismail,¹ Robert Drost,¹ Janis Siebrecht,¹ Haonan Huang,¹ and Christian R. Ast^{1,*}

¹Max-Planck-Institut für Festkörperforschung, Heisenbergstraße 1, 70569 Stuttgart, Germany

(Dated: September 23, 2022)

Electric control of spins has been a longstanding goal in the field of solid state physics due to the potential for increased efficiency in information processing. This efficiency can be optimized by transferring spintronics to the atomic scale. We present electric control of spin resonance transitions in single molecules by employing electron spin resonance scanning tunneling microscopy (ESR-STM). We find strong bias voltage dependent shifts in the ESR signal of about ten times its linewidth, which is due to the electric field induced displacement of the spin system in the tunnel junction. This opens up new avenues for ultrafast control of coupled spin systems, even towards atomic scale quantum computing, and expands on understanding and optimizing spin electric coupling in bulk materials.

INTRODUCTION

Spintronics and the concept to control spin and magnetic properties using electric fields have been on the forefront of solid state research for the past several decades with the promise to increase efficiency in data processing [1–4]. Different concepts have been considered such as the spin transistor [5–8], the spin Hall effect [9, 10], dopants in silicon [11–13], and magnetic molecules [14–22]. Specifically, spin-electric control allows for superior scalability and switching as electric fields are more easily contained and faster to manipulate than magnetic fields. This type of processing could be further optimized by transferring it to the atomic scale, for which scanning tunneling microscopy (STM) is an ideal platform in realizing such a goal. Specifically, the combination of electron spin resonance spectroscopy (ESR) with STM has expanded the sensitivity of ESR to atomic scale spin systems, and has enhanced the attainable energy resolution of STM well into the neV range [23–27].

As the manipulation capabilities in STM are mostly based on electrical control, implementing sizeable atomic scale electrical spin control can become not only possible with ESR-STM, but also quite effective. The applied bias voltage typically induces a very strong electric field between the tip and sample due to the extremely small gap of only a few Ångströms [28]. Moreover, ESR spectra are typically acquired by sweeping the microwave frequency or the magnetic field, so that the bias voltage essentially becomes a free parameter to be tuned. However, so far the bias voltage in ESR-STM has not been employed for spin manipulation.

In this study, we exploit the bias voltage as an electrical means for direct manipulation of spin transitions. We use a TiH molecule on an insulating MgO layer (see Fig. 1(a)) to demonstrate a direct tuning of the g -factor and the tip magnetic field. In this system, the resonance peak shifts by many line widths within a bias voltage range of 240 mV (see Fig. 1(b)), which is much stronger than what has been predicted for this system (on a different adsorption site) [29] or previously measured in bulk systems [15]. We explain this effect by the strong electric field in the tunnel junction induced by the applied bias voltage and felt by the dipolar TiH molecule.

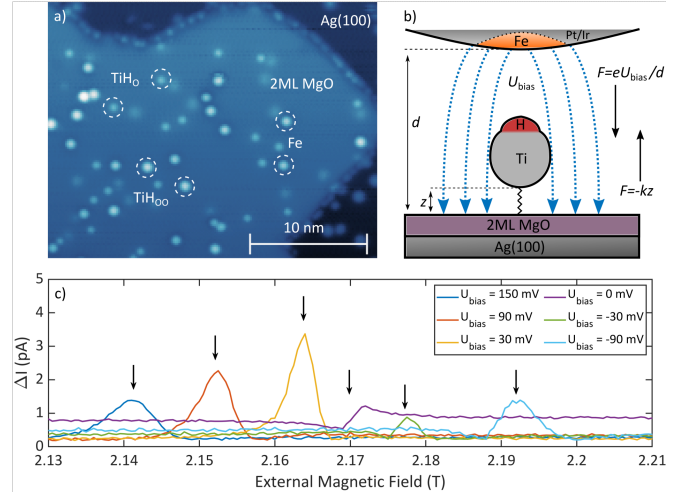


Figure 1: **ESR on TiH molecules** (a) STM topography of 2 ML MgO on a Ag(100) substrate decorated with individual TiH molecules and Fe atoms ($U_{\text{sp}} = 100$ mV, $I_{\text{sp}} = 20$ pA). The different species are labelled and circled accordingly. (b) Schematic of the tunnel junction during the ESR experiment. Force vectors representing the electric force induced by the bias voltage and elastic force of the Ti-MgO bond are shown. Additionally, the electric forces may act on the Ti-H bond. (c) Magnetic field sweeps performed at different STM junction bias voltages U_{bias} ($U_{\text{sp}} = 100$ mV, $I_{\text{sp}} = 250$ pA, $f_{\text{rf}} = 61.545$ GHz, $U_{\text{rf}} = 20$ mV). The ESR peak positions are labelled with black arrows.

A change in the electric force shifts the equilibrium position of the TiH molecule, resulting in the g -factor being modified and the molecule feeling a different magnetic field from the spin-polarized tip. The g -factor is, in part, modified due to a change in the crystal field felt by the TiH [29].

VOLTAGE DEPENDENT ESR-STM

The measurements were done on TiH molecules that adsorb on the bridge-site between two O atoms of the MgO double layer. They are labelled as TiH₀₀ in Fig. 1(a). Varying the bias voltage continuously, we observe the evolution of the ESR peak as a function of both bias voltage and external

magnetic field at a constant microwave radiation frequency of 61.545 GHz and a microwave amplitude of 20 mV. This is shown for two different setpoint currents of $I_{sp} = 100$ pA and $I_{sp} = 250$ pA in Fig. 2(a) and (b), respectively. Unless otherwise noted, the corresponding setpoint voltage is $U_{sp} = 100$ mV. The horizontal features in Fig. 2(a) and (b) are due to the interaction of the microwaves with the background density of states and are not related to the ESR signal [30–33]. Comparing the slope of the ESR peak in Fig. 2(a) and (b), we directly see that the change in the resonance condition is more pronounced for the higher setpoint current, which points towards an influence of the electric field rather than the bias voltage. We have obtained similar results for TiH molecules adsorbed on top of an O atom of the MgO layer (labeled TiH_O in Fig. 1(a)), which are presented in the Supplementary Information [34].

For a more quantitative analysis of the evolution of the ESR peak, we exploit the linear dependence of the ESR resonance on the magnetic field as

$$E_Z = h f_{res} = g \mu_B (B_{ext} + B_{tip}), \quad (1)$$

where E_Z is the Zeeman energy, f_{res} is the resonance frequency, g is the g -factor, and $B_{ext,tip}$ are the external magnetic field and the field of the tip felt by the spin system (henceforth the tip field), respectively. Furthermore, we assume the spin to be $S = 1/2$ [35], h is Planck's constant, and μ_B is the Bohr magneton. Both the tip field B_{tip} and the g -factor will be a function of the applied bias voltage. Analyzing the data at different frequencies, we extract the g -factor and the tip field B_{tip} dependency on the bias voltage at four different setpoint currents, which is shown in Fig. 2(c) and (d) (for details on the curve fitting, see the Supplementary Information [34]). We can clearly see that both the g -factor and the tip field B_{tip} monotonically increase with increasing bias voltage. This indicates that both quantities are sensitive to the changing electric field. In addition, the change is stronger at a larger setpoint current, which is consistent with our interpretation as a smaller tip-sample distance will lead to a stronger adjustment of the electric field with respect to bias voltage.

One notable difference in the behavior of the g -factor and the tip field B_{tip} is around zero bias voltage, where the effects of the electric field vanish. Interestingly, near zero bias voltage the tip field is relatively stagnant as a function of the set point current, while the increase in the g -factor is comparable to non-zero bias voltages. Calculations in the literature show that the g -factor increases as the molecule-substrate distance decreases for TiH_O [29, 36] (we expect a similar behavior for TiH_{OO}). We have measured approach curves demonstrating that the molecule-substrate coupling increases as the tip-sample distance is reduced. This indicates a decrease in the molecule-substrate distance, which provides an overall consistent behavior for the increasing g -factor for larger set point currents (see Supplementary Information for details [34]). Our findings show that adjusting the tip-sample distance results in changes to both the tip field and the g -factor. The changes due to the tip-sample distance have pre-

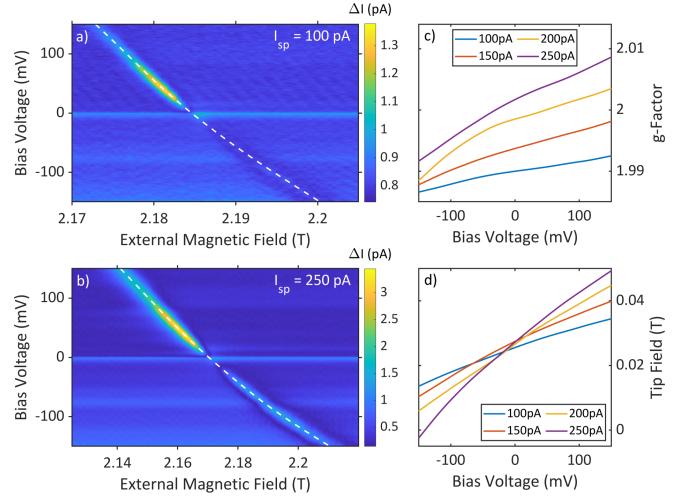


Figure 2: Voltage dependence of the ESR signal (a)-(b) Magnetic field/bias voltage sweeps performed at two different current set points ($U_{sp} = 100$ mV, $f_{rf} = 61.545$ GHz, $U_{rf} = 20$ mV, (a) $I_{sp} = 100$ pA, (b) $I_{sp} = 250$ pA). White dashed lines show a spline fit to the ESR peak positions as a function of bias voltage. (c)-(d) Extracted g -factor and tip field vs. bias voltage at four current set points.

viously been attributed to the tip field [35, 37, 38], while theoretical considerations of an electric field dependence have not taken changes in the tip field into account [29]. However, as we show here, the two effects cannot be easily separated.

To compare our results with literature, we calculate an effective frequency shift as a function of applied bias voltage of 0.83 GHz/V and 4.3 GHz/V for the g -factor and the tip field, respectively, at a setpoint current of 250 pA. These values are orders of magnitude larger than what has recently been reported for the ESR peak shift of 5.7 kHz/V in a bulk matrix of HoW₁₀ nanomagnets [15]. We can reach these values because the electric field becomes extremely large between the tip and sample. Comparing the spin-electric coupling (SEC) constants, which relate the frequency shift to the applied electric field, the situation looks a bit different. For the HoW₁₀ nanomagnets [15], a value of 11.4 Hz/(V/m) was reported, while we estimate values of 0.4 Hz/(V/m) and 2.2 Hz/(V/m) for the g -factor and the tip field B_{tip} , respectively, assuming a tip-sample distance of about 5 Å. While this indicates a more efficient coupling mechanism for the HoW₁₀ nanomagnets, the particular TiH system was not optimized *a priori* for high SEC, so we anticipate spin systems with superior SEC to be identified in the future.

Furthermore, the response of the Zeeman splitting to an electric field has been previously calculated specifically for the TiH molecule on MgO, albeit on an oxygen site TiH rather than on bridge site TiH [29]. The calculated frequency shift is estimated to be about 0.2 GHz/V, which is smaller than what we have observed experimentally. Neglecting the effect of the tip field, which was not considered in the calculations, we find a four times stronger change in the frequency shift

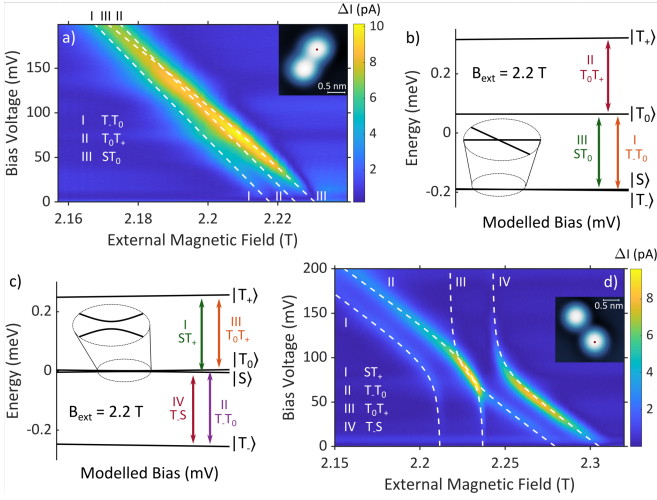


Figure 3: Interaction tuning in dimers (a) Magnetic field/bias voltage sweep on a strongly coupled dimer ($U_{\text{sp}} = 150$ mV, $I_{\text{sp}} = 1$ nA, $f_{\text{rf}} = 61.545$ GHz, $U_{\text{rf}} = 20$ mV). The inset shows the topography of the dimer with the red dot indicating the position of the tip during measurements ($U_{\text{sp}} = 100$ mV, $I_{\text{sp}} = 20$ pA). The white dashed lines are fits to the ESR peak positions corresponding to the transitions in panel (b). (b) Modelled behaviour of the spin states at a constant external magnetic field that result in the ESR transitions measured by the experiment in (a). The colored arrows show the observed transitions. (c) Modelled behaviour of the spin states at a constant external magnetic field that result in the ESR transitions measured by the experiment in (d). The colored arrows show the observed transitions. (d) Magnetic field/bias voltage sweep showing the avoided crossing of two coupled TiH molecules ($U_{\text{sp}} = 100$ mV, $I_{\text{sp}} = 400$ pA, $f_{\text{rf}} = 61.545$ GHz, $U_{\text{rf}} = 20$ mV). The inset shows the topography of the dimer with the red dot indicating the position of the tip during measurements ($U_{\text{sp}} = 100$ mV, $I_{\text{sp}} = 20$ pA). The white dashed lines are fits to the ESR peak positions corresponding to the transitions in panel (c).

for the g -factor in the experiment. We surmise that additional changes other than the crystal field gradient and the equilibrium position of the whole TiH molecule, such as a change in the Ti-H bond or simply the different adsorption site, contribute to this difference. The sensitivity of the TiH molecule to the local environment is already illustrated by changing the spin state from $\frac{3}{2}$ in the gas phase to $\frac{1}{2}$ upon adsorption on the surface, as well as changing the g -factor from about 2 to 0.6 by moving to a different binding site on the MgO [36, 39]. The ability now to tune the g -factor and the tip field B_{tip} by means of the bias voltage opens up an entirely new degree of freedom for *in situ* electrical manipulation of the spin transitions.

ELECTRIC CONTROL OF MULTIPLE SPINS

We demonstrate direct manipulation through SEC on two different types of dimers with different distances between the TiH molecules [35, 40]. In the first example, the two bridge site TiH molecules (TiH_{OO}) are 644 pm apart (see in-

set in Fig. 3(a)), such that the coupling is relatively strong ($J \approx 61.1$ GHz). We identify three transitions in this dimer in Fig. 3(a). These transitions (labeled I, II, and III) are well separated near zero bias voltage and subsequently broaden as well as intersect as we increase the bias voltage [40]. The white dashed lines are fits to a dimer spin Hamiltonian assuming a linear dependence of the g -factors and the tip field B_{tip} on the bias voltage (for details see the Supplementary Information [34]). The corresponding energy levels at a constant external field of 2.2 T are plotted in Fig. 3(b) with the transitions being indicated. We identify transition III as a clock transition that would not be visible if the two g -factors in the dimer were equal [40]. Therefore, we know that the two g factors are not equal even at zero bias voltage. Furthermore, as shown in Fig. 3(a) we can tune transitions II and III such that they are located at the same external magnetic field value, which demonstrates that we can manipulate the spin transitions in a dimer by means of SEC.

If the two TiH molecules are 1.04 nm apart (see inset in Fig. 3(d)), the interaction between them is reduced ($J \approx 0.67$ GHz), which shifts the energy of the singlet state $|S\rangle$ close to the triplet state $|T_0\rangle$ as shown in Fig. 3(c) [40, 41]. The singlet state $|S\rangle$ and the triplet state $|T_0\rangle$ undergo an avoided crossing (see inset in Fig. 3(c)), which can be observed experimentally [41]. We have tuned the tip-sample distance such that we can observe this avoided crossing in a bias voltage range between 0 mV and 200 mV as shown in Fig. 3(d). The four transitions that are visible in Fig. 3(d) are labelled I through IV corresponding to the transitions indicated in Fig. 3(c). We can clearly see how the two pairs of transitions associated with each TiH molecule in the dimer approach the avoided crossing and separate again. The white dashed lines are fits to the same dimer spin Hamiltonian as before, just with a weaker exchange interaction, which corroborates the experimental observations (for details on the parameters see the Supplementary Information [34]). For smaller magnetic fields below the avoided crossing, the transitions I and II are strongly influenced by the SEC, which indicates that the wave functions of the corresponding energy levels are located on the TiH molecule under the tip. As transitions III and IV are much less influenced by the applied bias voltage, we conclude that the corresponding wave functions are located on the TiH molecule next to the tip. The slope is not vertical, so we expect some influence of the electric field on the TiH molecule next to the tip about 1 nm away. For higher magnetic fields above the avoided crossing, the situation is reversed, such that the wave functions for transitions III and IV are in the TiH below the tip and the wave functions for transitions I and II are in the TiH next to the tip.

OPTIMIZING COHERENCE IN COUPLED SPIN STATES

The ability to manipulate spin interactions in dimers through SEC clearly demonstrates the versatility of voltage dependent ESR-STM. However, the tunneling current itself is

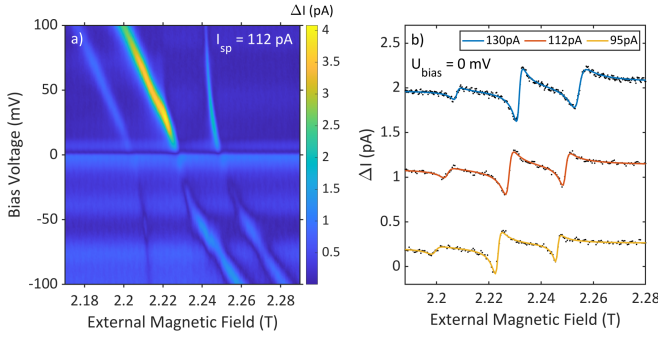


Figure 4: **Tuning the avoided crossing** (a) Magnetic field/bias voltage sweep showing the avoided crossing of the TiH dimer in Fig. 3(c) near zero bias voltage ($U_{sp} = 50$ mV, $I_{sp} = 112$ pA, $f_{rf} = 61.545$ GHz, $U_{rf} = 20$ mV). (b) ESR sweeps measured at zero bias showing how the resonances shift with respect to current set point ($U_{sp} = 50$ mV, $f_{rf} = 61.545$ GHz, $U_{rf} = 20$ mV). This shows that the tip-sample distance can be adjusted to bring the avoided crossing exactly to zero bias.

the biggest source of decoherence in the ESR excitation [42]. As a final proof-of-principle, we exploit both the bias voltage and the tip-sample distance as two degrees of freedom to move the avoided crossing to zero bias voltage, where the tunneling current is minimized and correspondingly the coherence time is maximized. This should enhance and maximize the coherent evolution of entangled states in a TiH dimer that has recently been demonstrated [41].

In order to move the avoided crossing of the second TiH dimer in Fig. 3(d) to zero bias voltage, we increase the tip-sample distance such that the setpoint reduces from $U_{sp} = 100$ mV and $I_{sp} = 400$ pA to $U_{sp} = 50$ mV and $I_{sp} = 112$ pA. Here, the avoided crossing shifts in bias voltage when adjusting the tip-sample distance, but essentially remains at the same position in external magnetic field. Fig. 4(a) shows the corresponding measurement, where the avoided crossing is now moved close to zero bias voltage. At zero bias voltage only the homodyne detection scheme allows to observe the ESR peaks, which typically appear as asymmetric peaks [40]. This can be seen in Fig. 4(b) for three different current setpoints, where the avoided crossing is above zero voltage (blue), near zero voltage (red), and below zero voltage (yellow). The shifts of the resonances corresponding to the movement of the avoided crossing in bias voltage is clearly visible. This demonstrates that by considering the bias voltage in ESR-STM, we can manipulate spin structures in a more complex manner than previously possible.

CONCLUSIONS

The ability to tune spin transitions at the nanoscale by means of an electric field opens up many new and interesting possibilities in the atomic manipulation capabilities of STM far beyond the proof-of-principle presented here. It adds the otherwise unconsidered bias voltage to the degrees of free-

dom for customizing spin systems to specific needs. In this regard, the tip-sample distance, which has previously been used, and the bias voltage present ideal tuning parameters for manipulating complex spin structures. Furthermore, the bias voltage opens avenues towards a more complete understanding of the ESR mechanism in the STM and its dynamics as well as its sources of decoherence and dissipation. This becomes particularly interesting for future applications in time-resolved experiments as it enables fast switching schemes for the bias voltage, which is not possible for magnetic fields or the tip-sample distance (e.g. coherent evolution [41], qubit operations [43, 44]). Looking on a broader perspective, we have established SEC in ESR-STM, which connects to the well established field of spintronics on an atomic scale. Moreover, studying the influence of the electric field within ESR-STM opens new possibilities and a better understanding for optimizing SEC in bulk materials.

ACKNOWLEDGEMENTS

The authors would like to thank Juan Carlos Cuevas, Andreas Heinrich, Klaus Kern, Jose Lado, Sander Otte, and Aparajita Singha for fruitful discussions. We are grateful to the European Research Council (ERC) for their financial support. This study was funded in part by the ERC Consolidator Grant AbsoluteSpin (Grant No. 681164) and by the Center for Integrated Quantum Science and Technology (IQST).

-
- * Corresponding author; electronic address: c.ast@fkf.mpg.de
- [1] F. Matsukura, Y. Tokura, and H. Ohno, *Control of magnetism by electric fields*, *Nature Nanotechnology* **10**, 209 (2015).
 - [2] B. E. Kane, *A silicon-based nuclear spin quantum computer*, *Nature* **393**, 133 (1998).
 - [3] M. Atzori and R. Sessoli, *The Second Quantum Revolution: Role and Challenges of Molecular Chemistry*, *Journal of the American Chemical Society* **141**, 11339 (2019).
 - [4] W. Eerenstein, N. D. Mathur, and J. F. Scott, *Multiferroic and magnetoelectric materials*, *Nature* **442**, 759 (2006).
 - [5] S. Datta and B. Das, *Electronic analog of the electro-optic modulator*, *Applied Physics Letters* **56**, 665 (1990).
 - [6] J. F. Gregg, I. Petej, E. Jouguet, and C. Dennis, *Spin electronics – a review*, *Journal of Physics D: Applied Physics* **35**, R121 (2002).
 - [7] A. Hirohata, K. Yamada, Y. Nakatani, I.-L. Prejbeanu, B. Diény, P. Pirro, and B. Hillebrands, *Review on spintronics: Principles and device applications*, *Journal of Magnetism and Magnetic Materials* **509**, 166711 (2020).
 - [8] S. Sugahara and J. Nitta, *Spin-Transistor Electronics: An Overview and Outlook*, *Proceedings of the IEEE* **98**, 2124 (2010).
 - [9] Y. K. Kato, R. C. Myers, A. C. Gossard, and D. D. Awschalom, *Observation of the Spin Hall Effect in Semiconductors*, *Science* **306**, 1910 (2004).
 - [10] J. Sinova, S. O. Valenzuela, J. Wunderlich, C. Back, and T. Jungwirth, *Spin Hall effects*, *Reviews of Modern Physics* **87**, 1213 (2015).

- [11] A. Laucht, J. T. Muhonen, F. A. Mohiyaddin, R. Kalra, J. P. Dehollain, S. Freer, F. E. Hudson, M. Veldhorst, R. Rahman, G. Klimeck, K. M. Itoh, D. N. Jamieson, J. C. McCallum, A. S. Dzurak, and A. Morello, *Electrically controlling single-spin qubits in a continuous microwave field*, *Science Advances* **1**, e1500022 (2015).
- [12] G. Tosi, F. A. Mohiyaddin, V. Schmitt, S. Tenberg, R. Rahman, G. Klimeck, and A. Morello, *Silicon quantum processor with robust long-distance qubit couplings*, *Nature Communications* **8**, 450 (2017).
- [13] S. Asaad, V. Mourik, B. Joecker, M. A. I. Johnson, A. D. Baczewski, H. R. Firgau, M. T. Mądzik, V. Schmitt, J. J. Pla, F. E. Hudson, K. M. Itoh, J. C. McCallum, A. S. Dzurak, A. Laucht, and A. Morello, *Coherent electrical control of a single high-spin nucleus in silicon*, *Nature* **579**, 205 (2020).
- [14] M. Trif, F. Troiani, D. Stepanenko, and D. Loss, *Spin-Electric Coupling in Molecular Magnets*, *Physical Review Letters* **101**, 217201 (2008).
- [15] J. Liu, J. Mrozek, A. Ullah, Y. Duan, J. J. Baldoví, E. Coronado, A. Gaita-Ariño, and A. Ardavan, *Quantum coherent spin-electric control in a molecular nanomagnet at clock transitions*, *Nature Physics* **17**, 1205 (2021).
- [16] J. Liu, J. Mrozek, W. K. Myers, G. A. Timco, R. E. Winpenny, B. Kintzel, W. Plass, and A. Ardavan, *Electric Field Control of Spins in Molecular Magnets*, *Physical Review Letters* **122**, 037202 (2019).
- [17] M. Fittipaldi, A. Cini, G. Annino, A. Vindigni, A. Caneschi, and R. Sessoli, *Electric field modulation of magnetic exchange in molecular helices*, *Nature Materials* **18**, 329 (2019).
- [18] J. Robert, N. Parizel, P. Turek, and A. K. Boudalis, *Polyanisotropic Magnetoelectric Coupling in an Electrically Controlled Molecular Spin Qubit*, *Journal of the American Chemical Society* **141**, 19765 (2019).
- [19] A. Palií, J. M. Clemente-Juan, B. Tsukerblat, and E. Coronado, *Electric field control of the optical properties in magnetic mixed-valence molecules*, *Chemical Science* **5**, 3598 (2014).
- [20] S. Cardona-Serra, J. M. Clemente-Juan, E. Coronado, A. Gaita-Ariño, N. Suaud, O. Svoboda, R. Bastardis, N. Guihéry, and J. J. Palacios, *Electrically Switchable Magnetic Molecules: Inducing a Magnetic Coupling by Means of an External Electric Field in a Mixed-Valence Polyoxovanadate Cluster*, *Chemistry – A European Journal* **21**, 763 (2015).
- [21] A. Gaita-Ariño, F. Luis, S. Hill, and E. Coronado, *Molecular spins for quantum computation*, *Nature Chemistry* **11**, 301 (2019).
- [22] C. Godfrin, A. Ferhat, R. Ballou, S. Klyatskaya, M. Ruben, W. Wernsdorfer, and F. Balestro, *Operating Quantum States in Single Magnetic Molecules: Implementation of Grover's Quantum Algorithm*, *Physical Review Letters* **119**, 187702 (2017).
- [23] S. Baumann, W. Paul, T. Choi, C. P. Lutz, A. Ardavan, and A. J. Heinrich, *Electron paramagnetic resonance of individual atoms on a surface*, *Science* **350**, 417 (2015).
- [24] W. Paul, S. Baumann, C. P. Lutz, and A. J. Heinrich, *Generation of constant-amplitude radio-frequency sweeps at a tunnel junction for spin resonance STM*, *Review of Scientific Instruments* **87**, 074703 (2016).
- [25] F. D. Natterer, F. Patthey, T. Bilgeri, P. R. Forrester, N. Weiss, and H. Brune, *Upgrade of a low-temperature scanning tunneling microscope for electron-spin resonance*, *Review of Scientific Instruments* **90**, 013706 (2019).
- [26] W. M. J. van Weerdenburg, M. Steinbrecher, N. P. E. van Mullekom, J. W. Gerritsen, H. von Allwörden, F. D. Natterer, and A. A. Khajetoorians, *A scanning tunneling microscope capable of electron spin resonance and pump-probe spectroscopy at mK temperature and in vector magnetic field*, *Review of Scientific Instruments* **92**, 033906 (2021).
- [27] R. Drost, M. Uhl, P. Kot, J. Siebrecht, A. Schmid, J. Merkt, S. Wünsch, M. Siegel, O. Kieler, R. Kleiner, and C. R. Ast, *Combining electron spin resonance spectroscopy with scanning tunneling microscopy at high magnetic fields*, *Review of Scientific Instruments* **93**, 043705 (2022).
- [28] C. Girard, C. Joachim, C. Chavy, and P. Sautet, *The electric field under a STM tip apex: implications for adsorbate manipulation*, *Surface Science* **282**, 400 (1993).
- [29] A. Ferrón, S. A. Rodríguez, S. S. Gómez, J. L. Lado, and J. Fernández-Rossier, *Single spin resonance driven by electric modulation of the g-factor anisotropy*, *Physical Review Research* **1**, 033185 (2019).
- [30] P. K. Tien and J. P. Gordon, *Multiphoton Process Observed in the Interaction of Microwave Fields with the Tunneling between Superconductor Films*, *Physical Review* **129**, 647 (1963).
- [31] P. Kot, R. Drost, M. Uhl, J. Ankerhold, J. C. Cuevas, and C. R. Ast, *Microwave-assisted tunneling and interference effects in superconducting junctions under fast driving signals*, *Physical Review B* **101**, 134507 (2020).
- [32] A. Roychowdhury, M. Dreyer, J. Anderson, C. Lobb, and F. Wellstood, *Microwave Photon-Assisted Incoherent Cooper-Pair Tunneling in a Josephson STM*, *Phys. Rev. Applied* **4**, 034011 (2015).
- [33] O. Peters, N. Bogdanoff, S. Acero González, L. Melischek, J. R. Simon, G. Reecht, C. B. Winkelman, F. von Oppen, and K. J. Franke, *Resonant Andreev reflections probed by photon-assisted tunnelling at the atomic scale*, *Nature Physics* **16**, 1222 (2020).
- [34] See Supplementary Information.
- [35] K. Yang, Y. Bae, W. Paul, F. D. Natterer, P. Willke, J. L. Lado, A. Ferrón, T. Choi, J. Fernández-Rossier, A. J. Heinrich, and C. P. Lutz, *Engineering the Eigenstates of Coupled Spin-1/2 Atoms on a Surface*, *Physical Review Letters* **119**, 227206 (2017).
- [36] M. Steinbrecher, W. M. J. van Weerdenburg, E. F. Walraven, N. P. E. van Mullekom, J. W. Gerritsen, F. D. Natterer, D. I. Badrtdinov, A. N. Rudenko, V. V. Mazurenko, M. I. Katsnelson, A. van der Avoird, G. C. Groenenboom, and A. A. Khajetoorians, *Quantifying the interplay between fine structure and geometry of an individual molecule on a surface*, *Physical Review B* **103**, 155405 (2021).
- [37] T. S. Seifert, S. Kovarik, C. Nistor, L. Persichetti, S. Stepanow, and P. Gambardella, *Single-atom electron paramagnetic resonance in a scanning tunneling microscope driven by a radio-frequency antenna at 4 K*, *Physical Review Research* **2**, 013032 (2020).
- [38] T. S. Seifert, S. Kovarik, P. Gambardella, and S. Stepanow, *Accurate measurement of atomic magnetic moments by minimizing the tip magnetic field in STM-based electron paramagnetic resonance*, *Physical Review Research* **3**, 043185 (2021).
- [39] A. Burrows, M. Dulick, J. C. W. Bauschlicher, P. F. Bernath, R. S. Ram, C. M. Sharp, and J. A. Milsom, *Spectroscopic Constants, Abundances, and Opacities of the TiH Molecule*, *The Astrophysical Journal* **624**, 988 (2005).
- [40] Y. Bae, K. Yang, P. Willke, T. Choi, A. J. Heinrich, and C. P. Lutz, *Enhanced quantum coherence in exchange coupled spins via singlet-triplet transitions*, *Science Advances* **4**, eaau4159 (2018).
- [41] L. M. Veldman, L. Farinacci, R. Rejali, R. Broekhoven, J. Gobeil, D. Coffey, M. Ternes, and A. F. Otte, *Free coherent evolution of a coupled atomic spin system initialized by electron scattering*, *Science* **372**, 964 (2021).
- [42] P. Willke, W. Paul, F. D. Natterer, K. Yang, Y. Bae, T. Choi, J. Fernández-Rossier, A. J. Heinrich, and C. P. Lutz, *Probing*

- quantum coherence in single-atom electron spin resonance*, [Science Advances](#) **4**, eaaq1543 (2018).
- [43] J. R. Petta, A. C. Johnson, J. M. Taylor, E. A. Laird, A. Yacoby, M. D. Lukin, C. M. Marcus, M. P. Hanson, and A. C. Gossard, *Coherent Manipulation of Coupled Electron Spins in Semiconductor Quantum Dots*, [Science](#) **309**, 2180 (2005).
- [44] Y. He, S. K. Gorman, D. Keith, L. Kranz, J. G. Keizer, and M. Y. Simmons, *A two-qubit gate between phosphorus donor electrons in silicon*, [Nature](#) **571**, 371 (2019).

Supplementary Material for Electric Control of Spin Transitions at the Atomic Scale

TIP AND SAMPLE PREPARATION

We cleaned Ag(100) in UHV by repeated cycles of Ar^+ ion sputtering at 5 kV and annealing at 820 K. MgO was grown on the clean Ag by simultaneous evaporation of Mg onto the sample surface, leaking of O_2 into the UHV space, and heating of the Ag substrate. Deposition times varied from 15 to 20 minutes with the Mg Knudsen cell being heated to 500 K, the O_2 being leaked to 10^{-6} mbar and heating of the Ag to 520 K. After the MgO growth, we deposited Fe and Ti on the surface using e-beam evaporators by applying an emission voltage of 850 V and an emission current of 8.5 mA for Fe and 19 mA for Ti. Furthermore, the sample was kept below 16 K during Fe and Ti deposition to ensure that the atomic species did not form clusters on the surface. The Ti species naturally hydrate due to the residual hydrogen gas found in the UHV space [1]. To create ESR sensitive tips we picked up between one and ten Fe atoms [2]. Dimers studied in this letter were either found naturally occurring on the sample or were created via atom manipulation [3].

MAGNETIC FIELD/BIAS VOLTAGE SWEEPS

We performed magnetic field/bias voltage sweeps on TiH molecules found on islands of MgO with a height of two monolayers (ML). Measurements were done by irradiating the junction at one frequency, and taking bias voltage dependent sweeps as a function of magnetic field. To minimize artifacts due to drift, we waited at least for two hours after approaching the tip and applying the microwave radiation prior to starting a sweep. To ensure that we do not drift off the molecular species under investigation, we performed atom tracking between bias sweeps while the magnetic field was ramping to the next value. In addition, we set the ramp rate of the magnet to relatively low values (≈ 2.5 mT/s), ensuring minimal heating and slow adjustment of the STM junction. During each bias sweep, atom tracking was turned off and the tip position was set to hold. Lastly, we modulated the radiation at a chopping frequency of 107 Hz and set the demodulation frequency of our lock-in amplifier to the same frequency. This way we can pick up the ESR signal of the system in the lock-in amplifier and increase our signal to noise ratio [4]. These sweeps took anywhere from four to twelve hours depending on the number of points being measured.

EXTRACTING g -FACTORS AND TIP FIELDS

To extract the bias voltage dependency of the g -factor and the magnetic field of the tip presented in the main text in Fig. 2, we measured magnetic field/bias voltage sweeps on a bridge site TiH molecule (TiH_{00}) at four different microwave frequencies (i.e. Zeeman energies) and four different current set points. Fig. S1 shows magnetic field/bias voltage sweeps at four different current set points. We keep the x-axis scaling the same in all panels to more clearly show the effect of the tip-sample distance on the bias voltage shift of the ESR signal. Already there is a clear indication that the spin-electric coupling (SEC) is stronger at smaller tip-sample distances. Fig. S2 shows magnetic field/bias voltage sweeps measured at four different microwave frequencies. The horizontal features in all panels of Figs. S2 and S9 are due to the interaction of the microwaves with the background density of states and not related to the ESR signal (cf. [5, 6]).

We can extract the dependencies of the g -factor and the tip field on the bias voltage at a specific current set point by the procedure outlined in Fig. S3. We extract the magnetic field positions of the ESR signal maxima at each bias voltage from a magnetic field/bias voltage sweep and do a spline fit of the bias voltage vs. magnetic field points as shown in Fig. S3(a). In practice, bias voltages smaller than ± 20 mV do not show a clear ESR signal, which we attribute to too low currents close to zero bias voltage. To bridge this gap, we interpolate the missing data points with a spline fit. We then use the spline fits at four different microwave frequencies and perform a

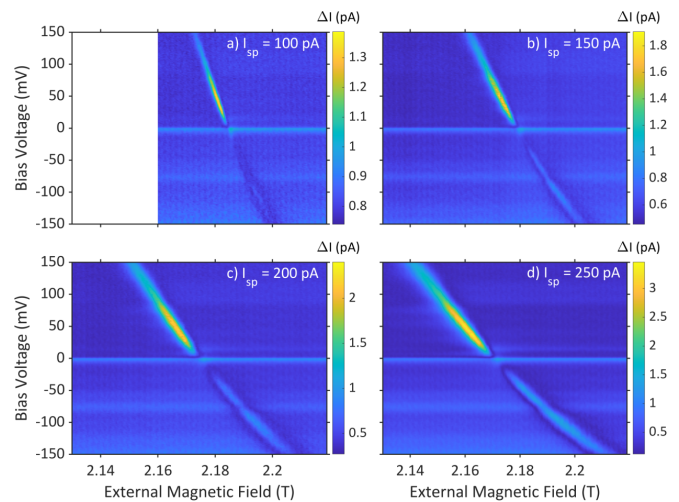


Figure S1: Magnetic field/bias voltage sweeps measured at different tip-sample distances ($U_{sp} = 100$ mV, $f_{rf} = 61.545$ GHz, $U_{rf} = 20$ mV, (a) $I_{sp} = 100$ pA, (b) $I_{sp} = 150$ pA, (c) $I_{sp} = 200$ pA, (d) $I_{sp} = 250$ pA)

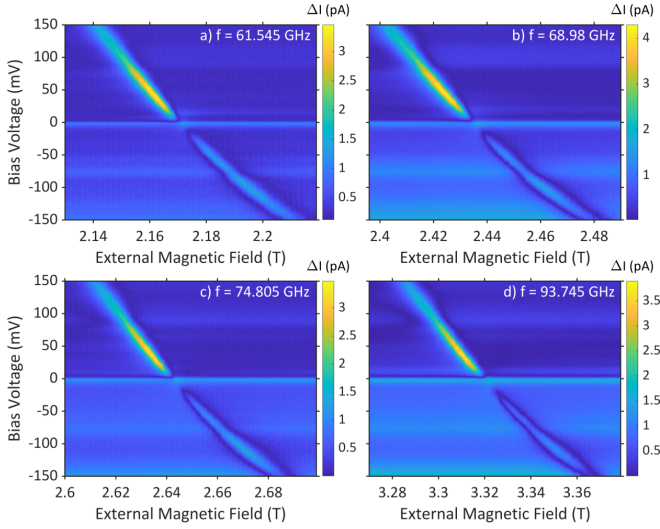


Figure S2: Magnetic field/bias voltage sweeps measured at different microwave frequencies ($U_{sp} = 100$ mV, $I_{sp} = 250$ pA, $U_{rf} = 20$ mV, (a) $f_{rf} = 61.545$ GHz, (b) $f_{rf} = 68.98$ GHz, (c) $f_{rf} = 74.805$ GHz, (d) $f_{rf} = 93.745$ GHz)

linear fit at each bias voltage. The spline fit data for each microwave frequency (i.e. Zeeman energy) is plotted in Fig. S3(b) along with a linear fit at two bias voltages (± 150 mV). Each linear fit yields the g -factor (slope) and the tip field B_{tip} (negative x -axis intercept) found at that bias voltage. From there, we can plot the dependency of the g -factor and tip field B_{tip} with respect to the bias voltage that we have presented in Fig. 2 of the main text.

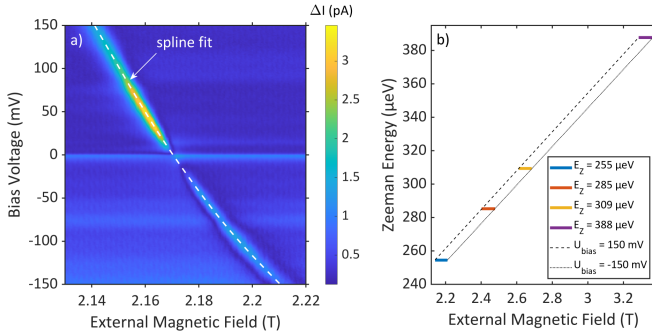


Figure S3: (a) Magnetic field/bias voltage sweep with a dashed line indicating the spline fit performed over the full bias voltage range. (b) Representation of the linear fits at each bias voltage to extract the bias voltage dependencies of the g -factor and tip field B_{tip} . Two linear fits are shown at 150 mV and -150 mV represented by the dashed and dotted lines, respectively.

To demonstrate the overall consistency of this multidimensional fit, we plot the extracted ESR peak positions along with the ESR resonance positions calculated from the fitted values, which are shown in Fig. S4 for all microwave frequencies and current setpoints. We see an overall good agreement and a continuous evolution. To illustrate the agreement quantitatively, we calculate the difference between the experimental

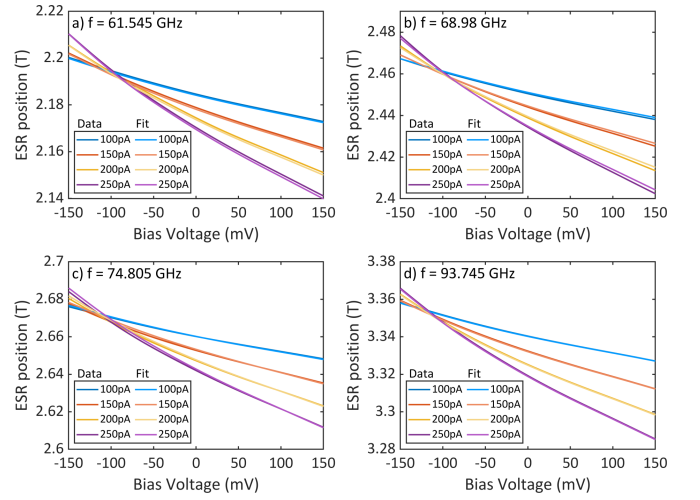


Figure S4: Comparison of the extracted ESR peak positions with the peak positions calculated from the fitted g -factors and tip fields B_{tip} . The different panels show the different microwave frequencies. We find generally good agreement for all frequencies and current setpoints.

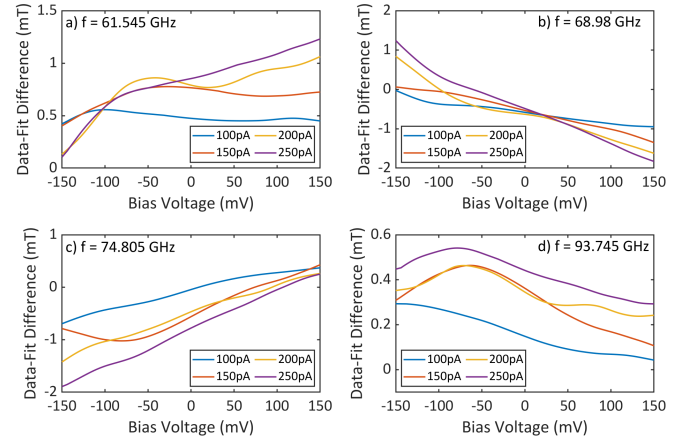


Figure S5: Differences between the extracted and the calculated ESR peak positions shown in Fig. S4. The deviations are always less than 2 mT indicating good overall agreement.

data and the modeled resonances, which is shown in Fig. S5 for the corresponding data in Fig. S4. We see that the deviations are generally small and never exceeding 2 mT. Therefore, we conclude that we have an overall consistent model.

TIP APPROACH

The coupling of the TiH molecule to the substrate can be inferred from the evolution of the tunnel junction transmission as a function of the tip sample distance. A similar situation has been analyzed previously in a different context [7]. Assuming that the TiH molecule is coupled to the substrate by the molecule-substrate coupling Γ_s and to the tip by the molecule-tip coupling Γ_t , the junction transmission τ can be

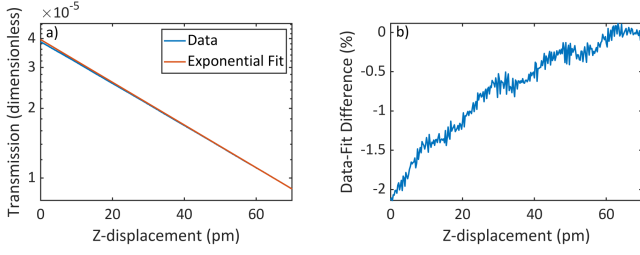


Figure S6: (a) Junction transmission as a function of z -displacement (tip-sample distance). The exponential fit is done in the low transmission regime revealing the sub-exponential evolution of the data. (b) Difference between data and fit normalized to the fit showing the sub-exponential evolution of the tip-approach.

written as [7, 8]

$$\tau = \frac{4\Gamma_s\Gamma_t}{(\Gamma_s + \Gamma_t)^2} \quad \Gamma_t \ll \Gamma_s \quad \frac{4\Gamma_t}{\Gamma_s}. \quad (\text{S1})$$

The transmission τ describes the junction conductance in units of the quantum of conductance $G_0 = 2e^2/h$, where e is the electron charge and h is Planck's constant. Since our junction is in the tunneling limit, i.e. $\Gamma_t \ll \Gamma_s$, we can easily see that a change in the molecule-substrate coupling Γ_s has a direct impact on the evolution of the junction transmission. We can reasonably assume that in the tunneling regime, the molecule-tip coupling Γ_t increases exponentially with decreasing tip-sample distance. If the molecule-substrate coupling Γ_s increases/decreases as the tip-sample distance decreases, the junction transmission τ will evolve less/more than exponentially, respectively. The tip approach for the tunnel junction measured in the main text in Fig. 2 is shown in Fig. S6(a). The blue line represents the data, while the red line represents an exponential fit to the data points at z -positions > 60 pm. A small but clear subexponential deviation of the data can be seen. The relative difference between data and fit is also plotted in Fig. S6(b) indicating that the junction transmission evolves below the fitted exponential evolution. From this behavior, we conclude that the molecule-substrate coupling Γ_s increases as the tip approaches the molecule. Therefore, it is likely that the molecule is pushed towards the surface in this approach range. This provides an overall consistent picture of an increasing g -factor as the molecule-substrate distance decreases [9] and explains the evolution of the g -factor at zero bias voltage for decreasing tip-sample distance.

MODELLING COUPLED SPINS

The models presented in Fig. 3(b) and (c) of the main text are based on a coupled spin Hamiltonian found in literature [1, 10, 11]:

$$H = -\mu_B(B_{\text{ext}} + B_{\text{tip}})g_1\hat{S}_1^z - \mu_B B_{\text{ext}}g_2\hat{S}_2^z + J\hat{S}_1 \cdot \hat{S}_2 + D(3\hat{S}_1^z\hat{S}_2^z - \hat{S}_1 \cdot \hat{S}_2). \quad (\text{S2})$$

	Avoided Crossing		Large J	
I_{sp}	400 pA	400 pA	1 nA	1 nA
U_{sp}	100 mV	100 mV	150 mV	150 mV
U_{bias}	0 mV	200 mV	0 mV	200 mV
J	0.669 GHz	0.669 GHz	61.11645 GHz	61.11645 GHz
D	13.3 MHz	13.3 MHz	50 MHz	50 MHz
g_1	1.92	1.925	2.0703	2.103
g_2	1.975	1.973	1.87	1.913
B_{tip}	0 mT	14 mT	20 mT	36 mT

Table SI: Fit parameters for the two dimers presented in the main text. The bias voltage values in the table are the extremal values at the edge of the interval. The parameters for the bias voltage values in between are linearly interpolated. The corresponding g -factors and tip fields differ between the dimers because they were measured with different tips and at different current and voltage set points I_{sp} and U_{sp} .

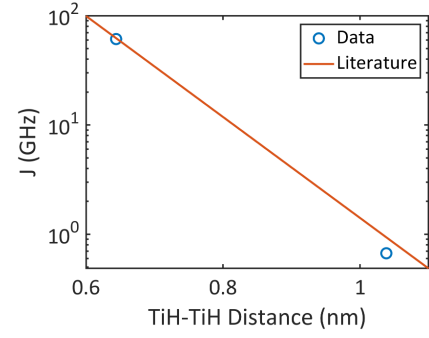


Figure S7: Comparison of the fit parameters for the exchange coupling J in the two dimers with the exponential dependence reported in literature [11].

This Hamiltonian works on the spin operators of the coupled spins, where g_1 and g_2 are the g -factors of the TiH molecule beneath the tip and beside the tip, respectively, B_{tip} is the tip field that is only considered to affect the TiH molecule beneath the tip, B_{ext} is the external magnetic field, J is the Heisenberg interaction energy between the two spins, and D is the dipole interaction between the two spins. For the dipole interaction, we estimate $D = 13.3$ MHz for the more distant dimer and $D = 50$ MHz for the closer dimer, which is a significantly smaller contribution than the other interactions.

Modelling of the experimentally observed transitions is done by considering the energy difference between two eigenvalues of the spin Hamiltonian. Modeling the TiH molecules as spin- $\frac{1}{2}$ systems, the spin Hamiltonian in Eq. (S2) can be diagonalized to analytically find the four eigenstates, three triplet states ($|T_+\rangle$, $|T_0\rangle$ and $|T_-\rangle$) and one singlet state ($|S\rangle$). In the case of the avoided crossing, we observe four transitions with energies: $|E_{T_0} - E_{T_-}|$, $|E_{T_0} - E_{T_+}|$, $|E_S - E_{T_-}|$, and $|E_S - E_{T_+}|$ [10, 12]. We then equate these energy differences to the energy hf of the microwave radiation, which

leads to the following set of equations:

$$hf = |E_{T_0} - E_{T_+}| = \frac{1}{2} [J + 2D + \mu_B(g_1(B_{\text{ext}} + B_{\text{tip}}) + g_2 B_{\text{ext}}) - \sqrt{(J - D)^2 + (\mu_B(g_1(B_{\text{ext}} + B_{\text{tip}}) + g_2 B_{\text{ext}}))^2}], \quad (\text{S3})$$

$$hf = |E_{T_0} - E_{T_-}| = \frac{1}{2} [J + 2D - \mu_B(g_1(B_{\text{ext}} + B_{\text{tip}}) + g_2 B_{\text{ext}}) - \sqrt{(J - D)^2 + (\mu_B(g_1(B_{\text{ext}} + B_{\text{tip}}) + g_2 B_{\text{ext}}))^2}], \quad (\text{S4})$$

$$hf = |E_S - E_{T_+}| = \frac{1}{2} [J + 2D + \mu_B(g_1(B_{\text{ext}} + B_{\text{tip}}) + g_2 B_{\text{ext}}) + \sqrt{(J - D)^2 + (\mu_B(g_1(B_{\text{ext}} + B_{\text{tip}}) + g_2 B_{\text{ext}}))^2}], \quad (\text{S5})$$

$$hf = |E_S - E_{T_-}| = \frac{1}{2} [J + 2D - \mu_B(g_1(B_{\text{ext}} + B_{\text{tip}}) + g_2 B_{\text{ext}}) + \sqrt{(J - D)^2 + (\mu_B(g_1(B_{\text{ext}} + B_{\text{tip}}) + g_2 B_{\text{ext}}))^2}]. \quad (\text{S6})$$

Using this set of equations we can solve for four different external magnetic fields B_{ext} ($B_{T_0 T_+}$, $B_{T_0 T_-}$, B_{ST_+} and B_{ST_-}) numerically using input values for J , D , g_1 , g_2 and B_{tip} . The microwave frequency f is a known input quantity. The resulting external magnetic field values B_{ext} represent the positions of the ESR peaks on the external magnetic field axis for the given transitions. In the case of the dimer with the stronger interaction energy, we model the positions of the ESR peaks by considering the following transition energies: $|E_{T_0} - E_{T_-}|$, $|E_{T_0} - E_{T_+}|$ and $|E_S - E_{T_0}|$ [11].

To incorporate the effect of the bias voltage in the modelling we assume a linearly dependence of g_1 , g_2 , and B_{tip} on the bias voltage in the range from 0 mV to 200 mV. This is based on the results presented in Fig. 2(c) and (d) of the main text. We find that to get accurate results, g_2 also has to shift with the bias voltage, which implies that the electric field of the tip still affects the TiH molecule next to the tip apex. This is to be expected as the tip and sample can be approximated as a plate capacitor close to the tip apex. Furthermore, we assume that J and D are not affected by the bias voltage. We choose the values for J according to the exponential distance dependence between the molecules in the dimer that has been established previously [1, 3, 11]. The comparison is shown in Fig. S7, where the red line is given by $J = J_0 \exp(-(r - r_0)/d)$ with $r_0 = 0.72$ nm, $d = 94$ pm, and $J_0 = 27.7$ GHz [3]. We then input a constant J and D into our set of equations and solve for the external magnetic field values B_{ext} constituting the positions of the ESR peaks as described above. For each set of g_1 , g_2 and B_{tip} , we solve for $B_{T_0 T_+}$, $B_{T_0 T_-}$, B_{ST_+} and B_{ST_-} for the case of the dimer with the avoided crossing, and $B_{T_0 T_+}$, $B_{T_0 T_-}$ and B_{ST_0} for the case of the dimer with a larger interaction energy. Finally, we superimpose the calculated ESR transitions over the data to find the

parameters with the best fit. The fit parameters g_1 , g_2 , B_{tip} , D and J for the two different dimers are presented in Table SI.

To plot the modelled eigenenergies in Fig. 3(b) and (c) of the main text, we simply input our estimated values for J and linearly changing g_1 , g_2 and B_{tip} into the diagonalized eigenenergies of Eq. (S2). Here, the x -axis in Fig. 3(b) and (c) is an “effective” bias voltage that we model with linearly shifting values for g_1 , g_2 and B_{tip} , but for a constant external magnetic field B_{ext} . Therefore, the evolution of the energy levels in Fig. 3(b) and (c) and the experimental data in Fig. 3(a) and (d) are not directly comparable.

MEASUREMENTS ON TiH₀

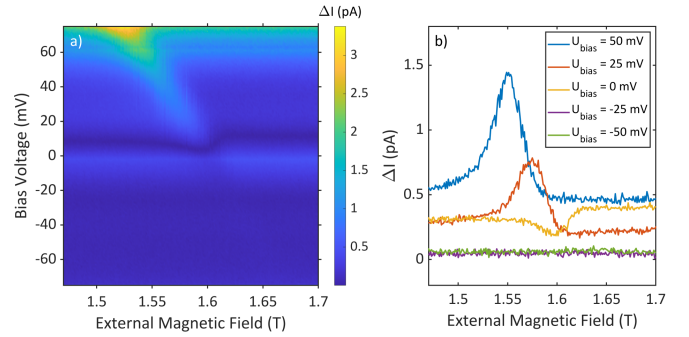


Figure S8: (a) Magnetic field/bias voltage sweep measured on a TiH₀ molecule ($U_{\text{sp}} = 100$ mV, $I_{\text{sp}} = 75$ pA, $f_{\text{rf}} = 19$ GHz, $U_{\text{rf}} = 20$ mV). (b) ESR sweeps measured on TiH₀ at different bias voltages. The evolution of the ESR peak shows a similar voltage dependence as for TiH₀₀, but the spin-electric coupling is stronger.

Magnetic field/bias voltage sweeps were also performed on on-site TiH molecules (TiH₀). Fig. S8(a) shows such a sweep where the ESR signal can be clearly seen. We see a linear shift of the ESR peak at positive bias voltages and no signal at negative bias voltages. We found that increasing the set point current of the magnetic field/bias voltage sweeps on TiH₀ increased the linear shift of the ESR signal with respect to the bias voltage, which is consistent with our observations on TiH₀₀ molecules. We found that the shift of the TiH₀ is much stronger than on the TiH₀₀ for similar set-point currents. We attribute this to the tip being closer to the sample when measuring on TiH₀ than when measuring on TiH₀₀. This is due to the smaller local density of states on the TiH₀ molecule, which leads to the tip sample distance being smaller on the TiH₀ than on the TiH₀₀ for comparable set points. This is supported by the different appearance of the TiH₀ compared to the TiH₀₀ as the TiH₀₀ molecules appear brighter than the TiH₀ molecules (cf. Fig. 1(a) of the main text).

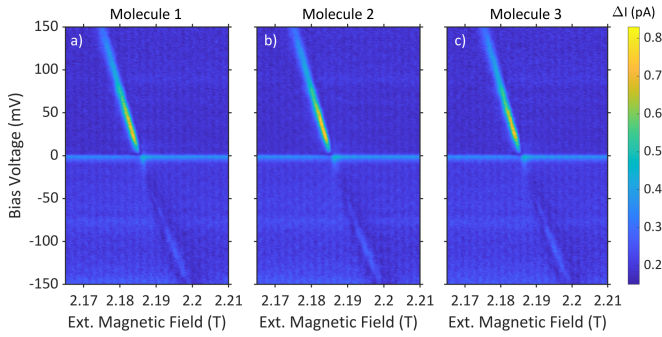


Figure S9: Magnetic field/bias voltage sweeps measured on three different TiH_{OO} molecules ($U_{\text{sp}} = 100 \text{ mV}$, $I_{\text{sp}} = 100 \text{ pA}$, $f_{\text{rf}} = 61.545 \text{ GHz}$, $U_{\text{rf}} = 20 \text{ mV}$). All three TiH_{OO} molecules show the same behavior.

SPIN-ELECTRIC COUPLING FOR DIFFERENT TIPS AND TiH_{OO} MOLECULES

As a consistency check we performed magnetic field/bias voltage sweeps on various TiH_{OO} molecules found on the sample with the same tip. Fig. S9 shows three such sweeps on three different TiH_{OO} molecules from which we conclude that the measurements are consistent and reproducible.

Furthermore, the data presented in the main text was measured using two different ESR-functionalized tips. The first tip was used for the measurements shown in Fig. 1, Fig. 2 and Fig. 3(a). The second tip was used in the avoided crossing measurements shown in Fig. 3(d) and Fig. 4. In addition, over the course of this study we have observed spin-electric coupling in the ESR signal for five tips. Lastly, during our experiments we never encountered an ESR tip nor a TiH molecule that did not show spin-electric coupling.

* Corresponding author; electronic address: c.ast@fkf.mpg.de

- [1] K. Yang, Y. Bae, W. Paul, F. D. Natterer, P. Willke, J. L. Lado, A. Ferrón, T. Choi, J. Fernández-Rossier, A. J. Heinrich, and C. P. Lutz, *Engineering the Eigenstates of Coupled Spin-1/2 Atoms on a Surface*, *Physical Review Letters* **119**, 227206 (2017).

- [2] S. Baumann, W. Paul, T. Choi, C. P. Lutz, A. Ardavan, and A. J. Heinrich, *Electron paramagnetic resonance of individual atoms on a surface*, *Science* **350**, 417 (2015).
- [3] K. Yang, S.-H. Phark, Y. Bae, T. Esat, P. Willke, A. Ardavan, A. J. Heinrich, and C. P. Lutz, *Probing resonating valence bond states in artificial quantum magnets*, *Nature Communications* **12**, 993 (2021).
- [4] T. S. Seifert, S. Kovarik, C. Nistor, L. Persichetti, S. Stepanow, and P. Gambardella, *Single-atom electron paramagnetic resonance in a scanning tunneling microscope driven by a radio-frequency antenna at 4 K*, *Physical Review Research* **2**, 013032 (2020).
- [5] P. K. Tien and J. P. Gordon, *Multiphoton Process Observed in the Interaction of Microwave Fields with the Tunneling between Superconductor Films*, *Physical Review* **129**, 647 (1963).
- [6] P. Kot, R. Drost, M. Uhl, J. Ankerhold, J. C. Cuevas, and C. R. Ast, *Microwave-assisted tunneling and interference effects in superconducting junctions under fast driving signals*, *Physical Review B* **101**, 134507 (2020).
- [7] H. Huang, R. Drost, J. Senkpiel, C. Padurariu, B. Kubala, A. L. Yeyati, J. C. Cuevas, J. Ankerhold, K. Kern, and C. R. Ast, *Quantum phase transitions and the role of impurity-substrate hybridization in Yu-Shiba-Rusinov states*, *Communications Physics* **3**, 199 (2020).
- [8] J. C. Cuevas and E. Scheer, *Molecular Electronics: An introduction to Theory and Experiment*, 2nd ed. (World Scientific, Singapore, 2017).
- [9] M. Steinbrecher, W. M. J. van Weerdenburg, E. F. Walraven, N. P. E. van Mullekom, J. W. Gerritsen, F. D. Natterer, D. I. Badrtdinov, A. N. Rudenko, V. V. Mazurenko, M. I. Katsnelson, A. van der Avoird, G. C. Groenenboom, and A. A. Khajetoorians, *Quantifying the interplay between fine structure and geometry of an individual molecule on a surface*, *Physical Review B* **103**, 155405 (2021).
- [10] L. M. Veldman, L. Farinacci, R. Rejali, R. Broekhoven, J. Gobeil, D. Coffey, M. Ternes, and A. F. Otte, *Free coherent evolution of a coupled atomic spin system initialized by electron scattering*, *Science* **372**, 964 (2021).
- [11] Y. Bae, K. Yang, P. Willke, T. Choi, A. J. Heinrich, and C. P. Lutz, *Enhanced quantum coherence in exchange coupled spins via singlet-triplet transitions*, *Science Advances* **4**, eaau4159 (2018).
- [12] X. Zhang, C. Wolf, Y. Wang, H. Aubin, T. Bilgeri, P. Willke, A. J. Heinrich, and T. Choi, *Electron spin resonance of single iron phthalocyanine molecules and role of their non-localized spins in magnetic interactions*, *Nature Chemistry* **14**, 59 (2022).